




## PAPER

Cite this: *Dalton Trans.*, 2018, **47**, 17055

## Slow magnetization dynamics in Co(II)/Co(III) triethanolamine/pivalate complexes†

Carolina Sarto,<sup>a</sup> Mathieu Rouzières,<sup>b,c</sup> Jun-Liang Liu,<sup>b,c</sup> Heiko Bamberger,<sup>d</sup> Joris van Slageren,<sup>d</sup> Rodolphe Clérac<sup>b,c</sup> and Pablo Alborés<sup>b,c</sup>    <sup>\*</sup>

We report the synthesis, structural characterization and a combined computational and experimental study of the magnetic properties of two pivalate cobalt complexes, a mononuclear Co(II) one and a tetranuclear Co(II)<sub>3</sub>Co(III) mixed valence polynuclear one. The latter shows SMM behaviour revealed under an applied DC field with a thermal barrier of *ca.* 30 cm<sup>-1</sup> competing with direct and Raman relaxation processes. The Orbach thermal barrier can be understood from the doublets energy ladder arising from the anisotropic exchange interaction among ground  $S_{\text{eff}} = 1/2$  of each Co(II) sites. The strong local zero-field splitting of the  $S = 3/2$  Co(II) states affords these well isolated ground Kramers doublets. DC and AC magnetic susceptibility measurements as well as HF-EPR spectra support this interpretation. CASSCF quantum chemical computations have been also performed in order to aid the overall comprehension of the magnetic behaviour in the reported complexes.

Received 8th October 2018,  
Accepted 12th November 2018

DOI: 10.1039/c8dt04041a

rsc.li/dalton

## Introduction

Paramagnetic compounds in which the individual molecules exhibit slow relaxation of their magnetization and magnetic bistability are known as single-molecule magnets (SMMs).<sup>1</sup> Since the discovery of the first SMM, in 1993,<sup>2</sup> an enormous amount of work has been done on these type of systems due to their potential applications in different relevant areas such as data storage devices,<sup>2b,3</sup> quantum computing,<sup>4</sup> spintronics<sup>5</sup> and also magnetic refrigeration at sub-Kelvin temperatures.<sup>6</sup> The main requisite for a molecule to behave as a SMM is its possibility to show magnetic bistability. For transition metal based SMM, this bistability can be induced by an energy barrier which is given by  $U_{\text{eff}} = |D|S^2$  or  $U_{\text{eff}} = |D|(S^2 - 1/4)$  for integer and half-integer ground states  $S$  total value, respectively (considering the following Hamiltonian;  $\hat{H} = D\hat{S}_z^2$ ). The  $D$  parameter is related to the axial magnetic anisotropy and splits the  $M_S$  sub-levels of the  $S$  ground state under zero magnetic field.<sup>1b</sup>

Transition-metal-based complexes showing SMM characteristics have been extensively reported during the last two decades;<sup>7</sup> among them the ones bearing Co(II) as metallic center<sup>8</sup> have been the less explored. However, there has been a renaissance, mainly of mononuclear Co(II) SMM, in the last years.<sup>9</sup> This renewed interest in Co(II) species relies on the ability of this ion to exhibit substantially large values of the  $D$  parameter, *i.e.* high magnetic anisotropy. Generally, the possibility that the local  $D$  tensors are not collinear, becomes a drawback to develop large reversal barriers.<sup>10</sup> On the other hand, a high versatility in modifying the coordination sphere around Co(II) sites can be found in polynuclear complexes and the overall content of Co(II) ions can also be changed by air-oxidation to their diamagnetic Co(III) congeners.

In this context, some of us have recently explored the reaction of the versatile triethanolamine (teaH<sub>3</sub>) ligand with a cobalt(II) pivalate (trimethylacetate = piv) precursor.<sup>11</sup> We have now extended this work to different experimental synthetic conditions, obtaining the new complexes: [Co<sup>II</sup>(teaH<sub>3</sub>)](piv) (**1**) and [Co<sup>II</sup>Co<sup>III</sup>(piv)<sub>5</sub>(teaH)<sub>2</sub>(teaH<sub>3</sub>)(H<sub>2</sub>O)<sub>2</sub>] (**2**). Herein we report their structural characterization and a combined computational and experimental study of their static and dynamic magnetic properties.

## Results and discussion

## Synthesis and structural characterization

As we and others have previously reported with other examples, the starting cobalt(II) complex, [Co<sub>2</sub>(μ-OH<sub>2</sub>)

<sup>a</sup>Departamento de Química Inorgánica, Analítica y Química Física/INQUIMAE (CONICET), Facultad de Ciencias Exactas y Naturales Universidad de Buenos Aires, Pabellón 2, Ciudad Universitaria, C1428EHA Buenos Aires, Argentina.  
E-mail: albores@qi.fcen.uba.ar; Fax: +5411/4576-3341

<sup>b</sup>CNRS, CRPP, UMR 5031, 33600 Pessac, France

<sup>c</sup>Univ. Bordeaux, CRPP, UMR 5031, F-33600 Pessac, France

<sup>d</sup>Institut für Physikalische Chemie, Universität Stuttgart, Pfaffenwaldring 55, D-70569 Stuttgart, Germany

† Electronic supplementary information (ESI) available. CCDC 1812496–1812497. For ESI and crystallographic data in CIF or other electronic format see DOI: 10.1039/c8dt04041a

( $\mu$ -piv)<sub>2</sub>(piv)<sub>2</sub>(Hpiv)<sub>4</sub>], can re-arrange in solution to afford higher nuclearity cobalt compounds and in this sense proves as a highly versatile synthetic precursor.<sup>11,12</sup> We have already examined this Co complex reaction with the simple triethanolamine ligand (teaH<sub>3</sub>) under open atmosphere, and were able to isolate different Co<sup>II</sup>/Co<sup>III</sup> polynuclear complexes.<sup>11</sup> We have now further explored the Co : teaH<sub>3</sub> stoichiometry ratio influence and the concentration effect over the final products in combination with the presence or not of a proton scavenger base as triethylamine, employing exclusively acetonitrile as solvent. We have also shown that when an excess (4 : 1) of teaH<sub>3</sub> with respect to {Co<sub>2</sub>} unit without the presence of the base (triethylamine) are mixed in acetonitrile, a {Co<sup>II</sup>Co<sup>III</sup>} complex is obtained. On the other hand, if a 2 : 1 ratio is employed in the presence of the proton scavenger, the obtained product is a {Co<sup>II</sup>Co<sup>III</sup>} compound.<sup>11</sup>

We have now explored the reaction with excess teaH<sub>3</sub> (also 4 : 1) but in a more concentrated acetonitrile solution and with addition of triethylamine. Under these conditions, the mononuclear cationic Co(teaH<sub>3</sub>)<sup>2+</sup> complex crystallized as the pivalate salt (**1**). These crystals appeared almost immediately, suggesting that the increased concentrations as well as the base favoured a kinetic product. If the same experimental conditions are kept but the teaH<sub>3</sub> : Co<sub>2</sub> ratio is lowered to 1 : 1, the obtained product is a neutral {Co<sup>II</sup>Co<sup>III</sup>} complex (**2**). When looking through this family of Co/piv/teaH<sub>3</sub> complexes, the following observation can be made about their Co(II) : Co(III) content: Co(II) is favoured over Co(III) through an increasing piv : teaH<sub>3</sub> ratio. This is due to the teaH<sub>3</sub> ability to stabilize the Co(III) oxidation state in contrast to pivalate stabilization of Co(II) state.

Compound **1** crystallizes in the triclinic  $P\bar{1}$  space group with two symmetry related pivalate anions and the +2 cationic mononuclear Co(II) complex in the unit cell. The molecular structure (Fig. 1) consists of a highly distorted octahedral

cobalt ion coordinated with two  $\kappa^3$ -N,O,O' teaH<sub>3</sub> ligands in a *fac* arrangement. The only three independent Co-ligand distances are Co(1)–O(1), 2.052(2) Å; Co(1)–O(2), 2.106(2) Å and Co(1)–N(1), 2.179(3) Å, with the four independent N–Co–O angles largely deviating from octahedral symmetry, 81.18, 82.85, 97.75 and 98.82 degrees. These geometrical parameters reveal a clear trigonal distortion, CShM value obtained with SHAPE<sup>13</sup> is 0.788 for an octahedral idealized geometry. A similar molecular structure was observed in the acetate salt of this Co(II) cationic complex crystallizing in an orthorhombic cell.<sup>14</sup> The pivalate counterions are held close to the complex through H-bond interactions with the coordinated O atoms of the teaH<sub>3</sub> ligands at both sides of the {CoO<sub>4</sub>} equatorial plane (see Fig. S11†). The non-coordinating O atoms of the teaH<sub>3</sub> ligands are involved in further H-interactions (coming in pairs) with pivalates allowing a supramolecular chainlike arrangements of Co(II) complexes (as well as pivalates) along *b*-axis direction (see Fig. S12†). This chain-like arrangement is not observed in the acetate example.

Complex **2** also crystallizes in the triclinic  $P\bar{1}$  space group with the entire molecule as the asymmetric unit. The molecular structure resembles two of the starting {Co<sub>2</sub>} moieties fused at a Co pair through a double  $\mu$ -O alkoxide and a *syn-syn*  $\mu$ -carboxylate bridges, with the final topology looking like a half ring (Fig. 2). No examples of {Co<sub>4</sub>} complexes showing this molecular arrangement have been reported so far. Net charge balance as well as Co–O bond distances allow to identify three Co(II) sites, Co(1), Co(2) and Co(3) and one Co(III) site, Co(4). Bond valence sums (BVS) further support these formal oxidation states (BVS: Co(1), 1.85; Co(2), 1.87; Co(3), 2.02 and Co(4), 2.87). The overall formula for complex **2**, matching the structural data is Co<sup>II</sup>Co<sup>III</sup>(teaH)<sub>2</sub>(teaH<sub>3</sub>)(piv)<sub>5</sub>(H<sub>2</sub>O)<sub>2</sub>.

The Co(III) site is triply bridged to both Co(2) and Co(3) sites, locally configuring a {Co(II)–Co(III)–Co(II)} triangular

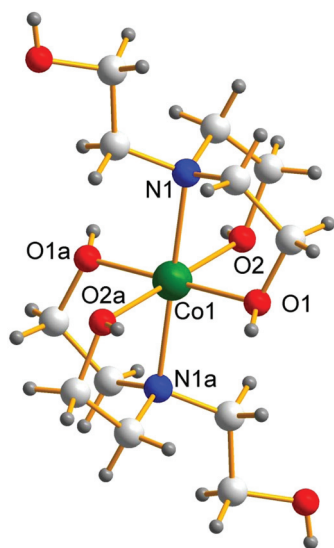


Fig. 1 Molecular representation of compound **1** in crystal structure. Symmetry equivalence operation, a:  $1 - x$ ,  $1 - y$ ,  $1 - z$ . Green: cobalt, red: oxygen, blue: nitrogen, light grey: carbon, dark grey: hydrogen.

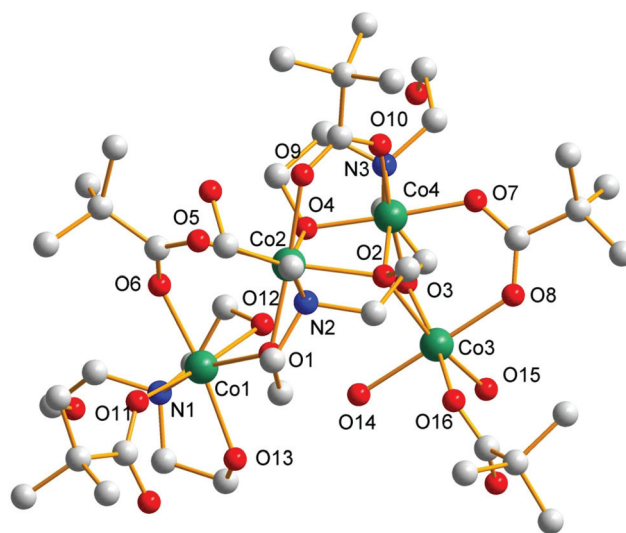


Fig. 2 Molecular representation of compound **2** in crystal structure. H atoms have been omitted for sake of clarity. Green: cobalt, red: oxygen, blue: nitrogen, light grey: carbon.

arrangement, with two clearly different Co(II) sites, a terminal one, further capped by aqua and pivalate ligands, and an inner one, additionally bridging the remaining Co(II) site (Co(1)) through a  $\mu$ -O alkoxide and a *syn-anti*  $\mu$ -carboxylate bridge. Local Co(III) environment is a distorted octahedron with Co–O distances ranging 1.862(3)–1.950(4) Å and a Co–N distance of 1.973(4) Å. CShM value for octahedral idealized geometry is 0.488.

The Co(II) sites are arranged in an angular configuration with a Co(1)–Co(2)–Co(3) angle of 88.4(2) degrees. The central Co(2) site is doubly bridged to the Co(1) through a  $\mu$ -alkoxide and a *syn-anti*  $\mu$ -carboxylate bridges and to the Co(3) site through a single  $\mu$ -alkoxide bridge. When looking at each of the six coordinated Co sites, it is easily noticed that all of them have quite different octahedral distorted coordination spheres. Co(1) has three pairs of distinct bond distances (all in *cis* arrangement): a shorter one, Co(1)–O(1), 2.013(3) Å; Co(1)–O(6), 2.026(4) Å, an intermediate, Co(1)–O(11), 2.082(5) Å; Co(1)–O(13), 2.158(4) Å and a longer one, Co(1)–O(12), 2.213(4) Å; Co(1)–N(1), 2.223(5) Å. Bond angles considerably deviate from pure octahedral ones, spanning a wide range of 76.6(2)–100.8(2) degrees. All these geometric parameters evidence at least a trigonal distortion. Regarding the Co(2) site, a different bond distances pattern is observed, two short Co–O bonds (*cis*), Co(2)–O(1), 2.048(4) Å; Co(2)–O(5), 2.056(5) Å, three intermediate Co–O bonds (*fac*), Co(2)–O(9), 2.109(4) Å; Co(2)–O(2), 2.122(3) Å; Co(2)–O(4), 2.129(3) Å and a longer Co–N bond, Co(2)–N(2), 2.192(4) Å. Bond angles considerably deviate from pure octahedral ones, spanning a wide range of 76.8(1)–101.4(2) degrees, similarly to Co(1) site. As the Co(1) site, this geometry suggests at least a trigonal distortion picture. Finally, the Co(3) site shows a bond distance pattern as follows: three short Co–O bonds (*mer*), Co(3)–O(3), 1.999(3) Å; Co(3)–O(16), 2.012(3) Å; Co(3)–O(8),

2.048(4) Å; two intermediate Co–O bonds (*cis*), Co(3)–O(14), 2.110(4) Å; Co(3)–O(15), 2.152(3) Å and a longer Co–O bond, Co(3)–O(2), 2.285(3) Å. As with the other Co(II) sites, bond angles deviate from octahedral ones spanning a range of 74.6(1)–101.0(2) degrees. Again, distortion at the Co(3) site is at best trigonal.

The CShM values of the three Co(II) sites are: Co(1), 1.464, Co(2), 1.232 and Co(3), 0.970, always for an octahedral idealized geometry.

A rich intra-molecular H-bond interaction pattern is observed, involving the aqua ligands and the non coordinated hydroxyl group from the teaH<sub>3</sub> ligand (see Fig. SI3†). Regarding the overall crystal packing, the aqua ligands play a main role in holding pairs of molecules in close contact due to multiple H-bond interactions between the four aqua ligands of both paired molecules (see Fig. SI4†). As a result the shortest intra-molecular Co...Co distance stands at 5.380(2) Å. Further H-bond interactions through the hydroxyl free teaH<sub>3</sub> ligand keeps the pair units in close contact.

## Magnetic properties

### DC magnetic data

Variable-temperature (1.8–300 K) DC magnetic susceptibility data at 1 kOe were recorded for complexes **1** and **2** (Fig. 3 and 4). In the case of mononuclear Co(II) complex **1**, the  $\chi T$  product at 300 K of 2.58 cm<sup>3</sup> K mol<sup>-1</sup> is clearly higher than the spin-only value ( $g = 2.0$ ) expected for a Co(II) ion with  $S = 3/2$  (1.87 cm<sup>3</sup> K mol<sup>-1</sup>). This is due to the orbital contribution of Co(II), which is known to be significant in an octahedral field and can be quenched by symmetry lowering.<sup>15</sup> In order to match the observed  $\chi T$  value at 300 K, the  $g$  value must be close to 2.35, indicating that orbital contribution in this case

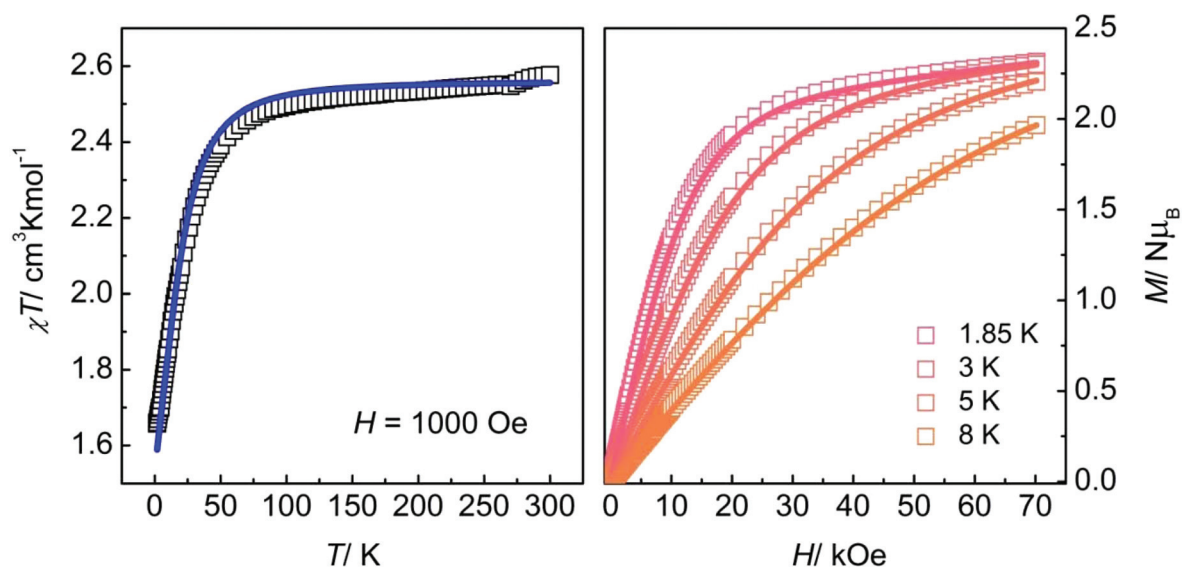


**Fig. 3** Left:  $\chi T$  vs.  $T$  data of compound **1** measured at 1000 Oe. Right:  $M$  vs.  $H$  in the range 1.85–8 K data of compound **1**. Open symbols correspond to experimental points and full line correspond to data fitting with  $g$  and  $D$  parameters and Hamiltonian of eqn (1) (see text).

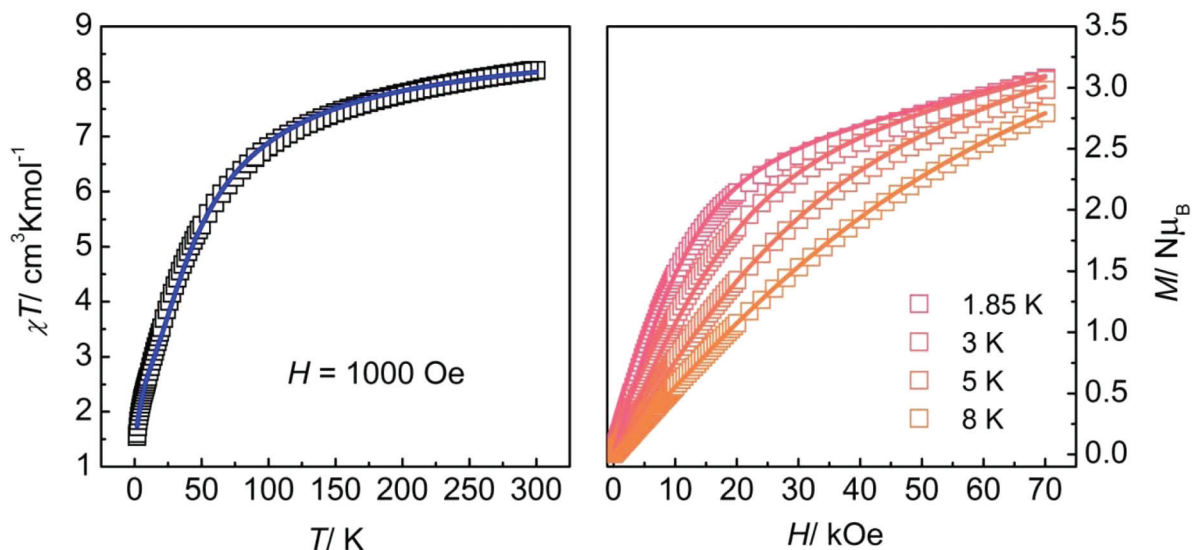


Fig. 4 Left:  $\chi T$  vs.  $T$  data of compound **2** measured at 1000 Oe. Right:  $M$  vs.  $H$  data in the range 1.85–8 K of compound **2**. Open symbols correspond to experimental points and full line correspond to fitting with  $g$ ,  $D$  and  $J$  parameters and Hamiltonian of eqn (2) (see text).

is relatively quenched (otherwise,  $g$  value typical rises up to 3 or more). On temperature lowering, the  $\chi T$  value remains essentially constant down to 50 K when it decreases to reach a final value of  $1.66 \text{ cm}^3 \text{ K mol}^{-1}$  at 1.85 K. This suggests the presence of a strong zero field splitting (ZFS) contribution, clearly expected for a Co(II) ion with quenched first order orbital magnetic moment contribution. In the case of complex **2**, the  $\chi T$  product at 300 K of  $8.20 \text{ cm}^3 \text{ K mol}^{-1}$  is also higher than the spin-only value ( $g = 2.0$ ) expected for three independent Co(II) ion with  $S = 3/2$  ( $5.625 \text{ cm}^3 \text{ K mol}^{-1}$ ). Here again, as discussed for complex **1**, the orbital contribution of Co(II) is responsible of this difference. If a  $g$  value of 2.41 is employed, good agreement with experimental value is observed, suggesting again a quenching of the orbital contribution to the magnetic moment of the Co(II) ions. Upon cooling,  $\chi T$  value continuously decreases to reach  $1.53 \text{ cm}^3 \text{ K mol}^{-1}$  at 1.85 K. This  $\chi T$  temperature dependence behaviour indicates dominating anti-ferromagnetic exchange interactions between the Co(II) ions in complex **2**. Of course, local ion ZFS contribution cannot be ruled out and is certainly contributing to the observed temperature dependence.

In order to gain more insight on the magnetic behaviour of these reported complexes, variable field and temperature magnetization data was acquired, in the range 1.8–8 K and 0–70 kOe external field (Fig. 3). The magnetization profile of complex **1** shows no superposition of the isotherms at maximum field and lowest temperature. Moreover, no complete saturation is achieved reaching a maximum magnetization value of  $2.31N\mu_B$  at 1.85 K and 70 kOe far away from the expected value of  $3.52N\mu_B$  ( $gS$  with  $g = 2.35$ ,  $S = 3/2$ ). This observations support the onset of a sizeable zero-field splitting of the ground state, as also evidenced by the susceptibility data. In the case of magnetization data profile of complex **2** (Fig. 4), steep raise is observed when lowering temperature and

increasing the field, to finally reach a smooth linear behaviour without saturation. A clear no superposition of the isotherms is also observed. This behaviour is due to the combined effect of local ion zero field splitting and exchange interactions, with probably low lying energy excited multiplets of higher spin state than the ground state.

In the case of complex **1**, the spin Hamiltonian employed for the simultaneous data fitting of susceptibility and magnetization data with PHI package<sup>16</sup> was:

$$\hat{H} = g\mu_B H \hat{S}_z + D \hat{S}_z^2. \quad (1)$$

This approach models an  $S = 3/2$  system with Zeeman and axial ZFS terms, employing naturally an isotropic  $g$  value for powder averaged measurements. Very good agreement is found with the following best fitting parameters:  $g = 2.34$  and  $D/hc = 23.1 \text{ cm}^{-1}$  (Fig. 3). If a negative value of  $D$  is attempted, no satisfactory enough simultaneous susceptibility and magnetization data fitting can be reached. The obtained  $g$  value, comparable with those of other reported Co(II) mononuclear six coordinated complexes,<sup>9a,c,f,i,j</sup> confirms the sizeable orbital momentum contribution quenching at first order. This quenching supports the validity of a spin-only Hamiltonian formalism and hence the extraction of the ZFS  $D$  parameter.

For fitting complex **2** experimental data, the presence of three Co(II) ions with potential exchange interactions must be properly handled. Hence, the following Hamiltonian was employed:

$$\hat{H} = g\mu_B H \sum_{i=1-3} \hat{S}_i + D \sum_{i=1-3} \hat{S}_{i,z}^2 - 2J(\hat{S}_1 \hat{S}_2 + \hat{S}_2 \hat{S}_3). \quad (2)$$

In spite of the fact that the spin topology requires two different exchange interaction  $J$  parameters (see Fig. 5), we kept a unique exchange constant in the HDvV spin

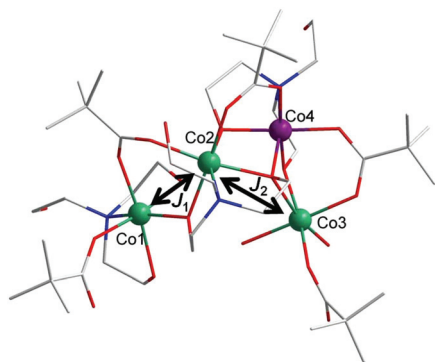


Fig. 5 Co(II) sites topology and main exchange interactions description in complex 2. Green: Co(II), violet: closed shell Co(III).

Hamiltonian term, in order to avoid over-parameterization. Indeed it is not possible to simultaneously fit susceptibility and magnetization data using only the exchange term and it is necessary to add a ZFS term, with a unique  $D$  parameter, again to avoid an over-parameterized model, as in principle the three Co(II) coordination spheres are different. Under all these simplifications, a quite reasonable theory/experience agreement is found with the following best fitting parameters (Fig. 4):  $g = 2.51$ ;  $J/hc = -5.0 \text{ cm}^{-1}$  and  $D/hc = 8.6 \text{ cm}^{-1}$  or alternatively with identical fitting quality (when switching  $D$  parameter sign)  $g = 2.49$ ;  $J/hc = -4.7 \text{ cm}^{-1}$  and  $D/hc = -7.1 \text{ cm}^{-1}$ . As observed in complex 1, the  $g$  value lower than 3.0, evidences a significant orbital momentum quenching. The  $D$  value has not a direct relationship with local Co(II) sites as the fitting approach imposed a unique value for all three different Co(II) ions. However it reflects a not negligible ZFS contribution as expected for this type of ion. The negative  $J$  exchange interaction parameter evidences an overall anti-ferromagnetic nature with a magnitude in agreement with the observed one in other reported  $\mu$ -carboxylate/ $\mu$ -alkoxide Co(II) complexes.<sup>11,12c,d,17</sup> Attempts to fit magnetization data with a model based on an isolated macro spin completely failed. This is understood considering that the  $D$  value shows the same order of magnitude (even higher) than the exchange  $J$  parameter, excluding the strong exchange coupled regime. The energy difference between the ground state doublet and first excited doublet that arises from the data fitting is only *ca.*  $12 \text{ cm}^{-1}$ .

### Quantum chemical calculations

In order to support all the experimental DC and AC magnetic data, we performed theoretical quantum chemical calculations through the ORCA package (3.0.2 release).<sup>18</sup> DFT broken symmetry methodology has proven successful in the study of other related Co(II) systems.<sup>11,12c,d</sup> In this case from three different broken symmetry (BS) spin topologies (see Fig. S15<sup>†</sup>) we have been able to extract the two distinct HDvV exchange coupling constants,  $J_{12}$ ,  $J_{13}$  (Table 2) which are not possible to obtain from experimental data due to over-parameterization limit-

ations. The obtained values confirm the anti-ferromagnetic nature and are in excellent agreement with experimental ones. We have previously established through a DFT-broken symmetry approach in a related Co(II) polynuclear complex, with a high degree of orbital contribution quenching, a clear magneto-structural correlation between the Co–O–Co angles and the isotropic  $J$  exchange coupling constant.<sup>11</sup> Here again, for complex 2, with Co–O–Co angles of  $116$  ( $J_{12}$ ) and  $130$  ( $J_{13}$ ) degrees, the correlation correctly predicts the antiferromagnetic  $J$  values between  $5$ – $10 \text{ cm}^{-1}$ .

Further insight into the magnetic anisotropy of complexes 1 and 2 were obtained using *ab initio* calculations. The axial and rhombic ZFS parameters ( $D$  and  $E$ ;  $\hat{H} = D\hat{S}_z^2 + E(\hat{S}_x^2 - \hat{S}_y^2)$ ) as well as the  $g$  tensors from the ground Kramers doublet were calculated (Table 2) using complete-active-space second-order perturbation theory (CAS\_NEVPT2) considering the effect of the dynamical electronic correlation based on complete-active-

Table 1 Crystallographic data for complexes 1 and 2

	1	2
Empirical Formula	C <sub>22</sub> H <sub>48</sub> CoN <sub>2</sub> O <sub>10</sub>	C <sub>43</sub> H <sub>90</sub> Co <sub>4</sub> N <sub>3</sub> O <sub>21</sub>
Formula weight	559.55	1220.89
$T$ (K)	170(2)	170(2)
Crystal system	Triclinic	Triclinic
Space Group	$P\bar{1}$	$P\bar{1}$
$a$ (Å)	6.4672(8)	11.9064(7)
$b$ (Å)	9.7445(15)	15.7978(9)
$c$ (Å)	11.8519(17)	15.8174(9)
$\alpha$ (°)	90.853(12)	87.099(5)
$\beta$ (°)	105.314(12)	71.868(5)
$\gamma$ (°)	107.173(12)	82.971(5)
$V$ (Å <sup>3</sup> )	684.76(18)	2805.9(3)
$Z$	1	2
$D_{\text{calc}}$ (mg m <sup>-3</sup> )	1.357	1.445
Absorption coefficient (mm <sup>-1</sup> )	0.680	1.235
$F(000)$	301	1290
$\lambda$ (Å)	0.71073	0.71073
$\theta$ range data collection (°)	3.53–27.0	3.52–27.0
Index ranges	$-8 \leq h \leq 7$ $-12 \leq k \leq 11$ $-15 \leq l \leq 15$	$-14 \leq h \leq 15$ $-20 \leq k \leq 19$ $-20 \leq l \leq 20$
Reflections collected/unique	4833/2923	34 669/12 103
$R_{\text{int}}$	0.0723	0.0834
Observed reflections [ $I > 2\sigma(I)$ ]	2513	8617
Completeness (%)	99.7	99.7
Maximum/minimum transmission	1.000/0.689	1.000/0.799
Data/restraints/parameters	2923/2/166	12 103/97/646
Goodness-of-fit (GOF) on $F^2$	1.079	1.081
Final $R$ -index [ $I > 2\sigma(I)$ ]/all data	0.0684/0.0776	0.0847/0.1150
wR index [ $I > 2\sigma(I)$ ]/all data	0.1723/0.1917	0.2199/0.2517
Largest peak and hole (e Å <sup>-3</sup> )	1.252 and $-1.604$	2.440 and $-1.499$
Weights, $w$	$1/[\sigma^2(F_o^2) + (0.1089P)^2 + 0.0699P]$ where $P = (F_o^2 + 2F_c^2)/3$	$1/[\sigma^2(F_o^2) + (0.1106P)^2 + 13.880P]$ where $P = (F_o^2 + 2F_c^2)/3$

**Table 2** Experimental and *ab initio* calculated spin Hamiltonian parameters of reported complexes (for details on calculations and fitting refer to text)

		Experimental			<i>Ab initio</i> calculated						
		$g^a$	$g$		$g$						
		DC magnetic data	HF-EPR data		$D/hc^a$ (cm <sup>-1</sup> )	Lowest energy KD		$D/hc$ (cm <sup>-1</sup> )	$E/D$		
1		2.34	2.88 <sup>b</sup>	3.15 <sup>c</sup>	1.91 <sup>d</sup>	23.1	1.46	16.1	0.27		
			1.79	2.15	3.51		2.00				
			1.93	1.93	5.61		6.75				
		Experimental			<i>Ab initio</i> calculated						
		$g$	$g$	$J/hc$ (cm <sup>-1</sup> )		$g$					
		DC magnetic data	HF-EPR data <sup>g</sup>	Isotropic <sup>e</sup>	Anisotropic <sup>f</sup> $J_x, J_y, J_z$	$D/hc$ (cm <sup>-1</sup> )	Lowest energy KD	$J_1/hc$ (cm <sup>-1</sup> )	$J_2/hc$ (cm <sup>-1</sup> )	$D/hc$ (cm <sup>-1</sup> )	$E/D$
2			Co1				Co1			Co1	
			1.87				2.02			16.6	0.11
			4.93				3.59				
			6.28				5.35				
		2.51 <sup>e</sup>	Co2	-5.0			Co2			Co2	Co2
		2.49	1.79	( $D > 0$ )	11.0		1.08			-32.5	0.18
		3.80 <sup>f</sup>	2.29		11.0	8.6 <sup>e</sup>	1.33	-6.8	-4.3		
			6.22		-32.0	-7.1	7.42				
				( $D < 0$ )						Co3	Co3
			Co3				Co3			-49.3	0.023
		1.14				0.16					
		0.95				0.17					
		6.07				7.94					

<sup>a</sup> DC magnetic data,  $S = 3/2$  model. <sup>b</sup> HF-EPR data,  $S = 3/2$  model with ZFS  $D$  parameter fixed at DC magnetic data value. <sup>c</sup> HF-EPR data,  $S = 3/2$  model with ZFS  $D$  parameter fixed at *ab initio* calculated value. <sup>d</sup> HF-EPR data,  $S_{\text{eff}} = 1/2$  model. <sup>e</sup> DC magnetic data with  $\pm|D|$  values. <sup>f</sup> DC magnetization data, exchange coupled  $S_{\text{eff}} = 1/2$  model. <sup>g</sup> HF-EPR data, exchange coupled  $S_{\text{eff}} = 1/2$  model.

space self-consistent field (CASSCF). In the case of complex **1**, the found value for the  $D$  parameter is in excellent agreement with the experimental value arising from DC magnetic data. The calculated strong rhombicity cannot be further experimentally tested; however the simulated DC magnetic data with the calculated  $D$  and  $E/D$  parameters are in very reasonable agreement with experiment (see Fig. SI6†). The same conclusion can be drawn with the  $g$  tensor main values of the ground Kramers doublet, whose isotropic  $g$  factor is in good agreement with the estimation arising from DC magnetic data best fitting parameters.

In the case of complex **2**,  $D$  and  $E/D$  parameters were calculated individually for each Co(II) center. Here it is not straightforward to compare these calculated parameters with the ones arising from DC magnetic data, where the fitting was performed fixing a unique  $D$  parameter for the three Co(II) sites together with, also a unique, exchange interaction parameter. Furthermore, the calculated  $D$  tensors are not collinear neither the  $g$  tensors of the Kramers ground doublet (Fig. 6). As the calculated Co(II) local  $D$  parameters are in the range of 10–30 cm<sup>-1</sup>, a picture of interacting isolated Kramers ground doublets with highly anisotropic  $g$  tensors can be reasonably

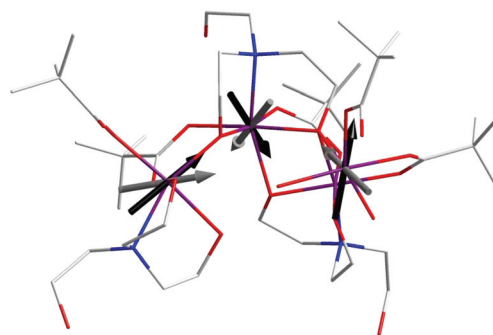


**Fig. 6**  $g$ -Tensors orientation of Co(II) sites ground doublets (gray) and  $D$ -tensors orientation (black), as arising from *ab initio* quantum chemical computations (see text), within compound **2** molecular structure.

employed for the interpretation of the low temperature data. In fact, it is possible to fit the magnetization data, alternatively, through the simplest spin Hamiltonian considering three interacting  $S_{\text{eff}} = 1/2$  sites, *i.e.* with a unique isotropic  $g$  factor and an axial exchange interaction tensor (eqn (3), see ESI†).

$$\hat{H} = g\mu_B H \sum_{i=1-3} \hat{S}_{\text{eff},i} - 2J_z(\hat{S}_{z,\text{eff},1}\hat{S}_{z,\text{eff},2} + \hat{S}_{z,\text{eff},2}\hat{S}_{z,\text{eff},3}) - 2J_{x,y}(\hat{S}_{x,\text{eff},1}\hat{S}_{x,\text{eff},2} + \hat{S}_{x,\text{eff},2}\hat{S}_{x,\text{eff},3} + \hat{S}_{y,\text{eff},1}\hat{S}_{y,\text{eff},2} + \hat{S}_{y,\text{eff},2}\hat{S}_{y,\text{eff},3}) \quad (3)$$

Several best fitting parameter combination can be found. If the  $g$  factor is constrained around the isotropic mean value from calculated ground Kramers doublets  $g$  tensors (between 3.8–4.6), the following parameters result:  $g = 3.8$ ,  $J_z/hc = -32 \text{ cm}^{-1}$  and  $J_{x,y}/hc = 11 \text{ cm}^{-1}$ . These values afford an isotropic exchange constant of antiferromagnetic nature, in agreement with the previously discussed DC magnetic data treatment. The energy difference between ground state doublet and first excited doublet arising from these best fitting parameters is *ca.*  $35 \text{ cm}^{-1}$ .

### HF-EPR spectroscopy

To get a better insight about the low lying levels energy splitting of the reported complexes, variable-frequency HF-EPR measurements were carried out. The spectra were measured on powder pellets of both complexes **1** and **2** at different temperatures and frequencies.

Complex **1** spectrum shows the expected pattern for an  $S = 3/2$  spin with a  $D$  parameter much higher than the microwave source and a rhombic  $g$  tensor, even at the highest explored frequency of 620 GHz, equivalent to  $20.7 \text{ cm}^{-1}$  (Fig. 7). This means that a lower limit for  $D$  parameter value can be established around *ca.*  $10 \text{ cm}^{-1}$ . The temperature dependence of the HF-EPR lines at 320 GHz, showing lower intensities for increasing temperature, supports a positive value for the  $D$  parameter, hence a  $|\pm 1/2\rangle$  ground doublet (see Fig. S18†). This result is in agreement with the experimental DC magnetic data and also with the quantum chemical calculations. Thus, EPR spectra can be well simulated as an effective  $S = 1/2$  with a rhombic  $g$  tensor (Fig. 7). The obtained  $g$  principal values are in

good agreement with the *ab initio* computed, supporting the high rhombicity at the Co(II) site (Table 2). Satisfactory simulations can alternatively be obtained with an  $S = 3/2$  model and experimental DC magnetic data ZFS parameter or quantum chemical calculated ZFS parameters (see Fig. S19 and S110†).

The HF-EPR spectra of complex **2** appear more complicated with two main resonances and several additional broad ones, depending on the microwave frequency (Fig. 8). Quantum chemical computations suggest isolated  $S_{\text{eff}} = 1/2$  at each Co(II) site due to strong ZFS contribution to the ground state  $S = 3/2$ . Hence it is possible to expect the EPR resonances arising from these three exchange coupled  $S_{\text{eff}} = 1/2$  doublets. However the main quantization axes of the  $g$  tensors of these Kramers doublets are not collinear, making difficult the EPR simulation. In fact, the number of possible parameters for a complete spin Hamiltonian in this case is definitely large. A possible approach, in a simplified picture, is to employ the calculated  $g$  tensors values as reference values and include the anisotropic exchange parameters obtained from low temperature DC magnetization data (eqn (5)).

$$\hat{H} = \mu_B \sum_{i=1-3} \vec{g}_i \hat{S}_{\text{eff},i} \vec{H} - 2J_z(\hat{S}_{z,\text{eff},1}\hat{S}_{z,\text{eff},2} + \hat{S}_{z,\text{eff},2}\hat{S}_{z,\text{eff},3}) - 2J_{x,y}(\hat{S}_{x,\text{eff},1}\hat{S}_{x,\text{eff},2} + \hat{S}_{x,\text{eff},2}\hat{S}_{x,\text{eff},3} + \hat{S}_{y,\text{eff},1}\hat{S}_{y,\text{eff},2} + \hat{S}_{y,\text{eff},2}\hat{S}_{y,\text{eff},3}) \quad (4)$$

Within this approximation, it is possible to get reasonable simulations for the HF-EPR spectra at the different measured frequencies (Fig. 8). The obtained values are in agreement with experimental DC magnetization data at low temperature and also in reasonable agreement with the calculated *ab initio*  $g$  tensors values considering their lack of collinearity (see Table 2). The expected broadening of the upper field reso-

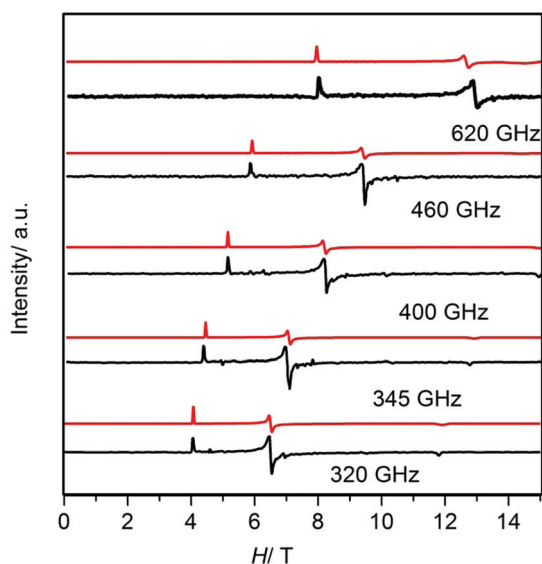


Fig. 7 HF-EPR spectra measured at 5 K and variable microwave frequency of a compound **1** powder sample. Black: experimental; Red: simulated (see text, 3 mT linewidth, and 0.04  $g$ -strain).

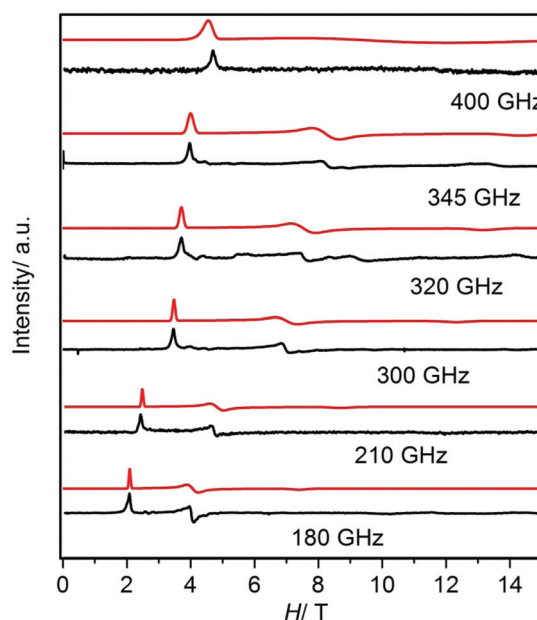


Fig. 8 HF-EPR spectra measured at 5 K and variable microwave frequency of a compound **2** powder sample. Black: experimental; Red: simulated (see text, 7 mT linewidth, and 0.12  $g$ -strain).

nance when increasing frequency can be reproduced through an appropriate  $g$ -strain. Hence it is possible to match the HF-EPR results with low temperature DC magnetic behavior with the aid of the quantum chemical computations. It must be remarked that the complete picture is more complicated than this simplified interpretation, mainly due to the non-colinearity of the local ground state doublets.

### AC magnetic data

In order to test for possible magnetization slow relaxation, AC susceptibility data were collected at low temperature at driving frequencies up to 10 kHz at zero DC external applied field and also with small applied fields up to 10 kOe. No out of phase signal was observed in the case of mononuclear complex **1** even under applied field (see Fig. SI11†). A possible explanation would be the existence of fast quantum tunnelling relaxation due to contribution of high transversal components in the Hamiltonian (*cf.* quantum computed  $E/D$  large value, almost at the  $1/3$  limit). Also in the case of compound **2**, no out of phase signal can be observed at zero DC-external field (see Fig. SI12†). However, slow magnetization relaxation is revealed under an applied DC field, as evidenced by the maximum observed in the out-of-phase susceptibility signal when scanning frequency and temperature (Fig. SI13†). The maximum shift supports the SMM (single-molecule magnet) behaviour of this complex. The DC field scanning of the AC susceptibility shows that the maximum out-of-phase signal at the lowest characteristic frequency is found at 1500 Oe (see Fig. SI13†), hence a detailed frequency and temperature dependence

data set was collected under this extremum applied field (Fig. 9). A single maximum is observed for the  $\chi''$  vs.  $T$  and  $\chi''$  vs. frequency profiles, suggesting the existence of a unique slow relaxation process. Employing the generalized Debye model, the characteristic relaxation time at each different temperature can be extracted. These data allows making an Arrhenius like plot and analyze the possible magnetization relaxation mechanisms operative for this complex.

When  $\ln \tau$  vs.  $T^{-1}$  is plot, the existence of the Orbach relaxation mechanism is strongly suggested by a linear regime. When large deviations are observed other possible mechanism must be considered like Raman processes or temperature independent quantum tunnelling (QT) ones. Under external DC applied field also the direct process can be relevant. In the case of complex **2**, a linear thermally activated regime is not easily identified (Fig. 10); hence all different contributions must be explored. In order to avoid a severe over-parameterization, we performed a simultaneous data fitting of relaxation time vs. temperature data at 1500 Oe and relaxation time vs. applied DC field at 2 K. An overall description of the relaxation time field and temperature dependence for a Kramers system is accounted by the following equation:

$$\frac{1}{\tau} = \frac{1}{\tau_0} \exp\left(-\frac{U_{\text{eff}}}{kT}\right) + C \left(\frac{1 + C_1 H^2}{1 + C_2 H^2}\right) T^n + A_1 H^4 T + \frac{B_1}{1 + B_2 H^2} \quad (5)$$

where each term represents the Orbach, Raman, Direct and QT mechanisms respectively. We found that the best agreement with

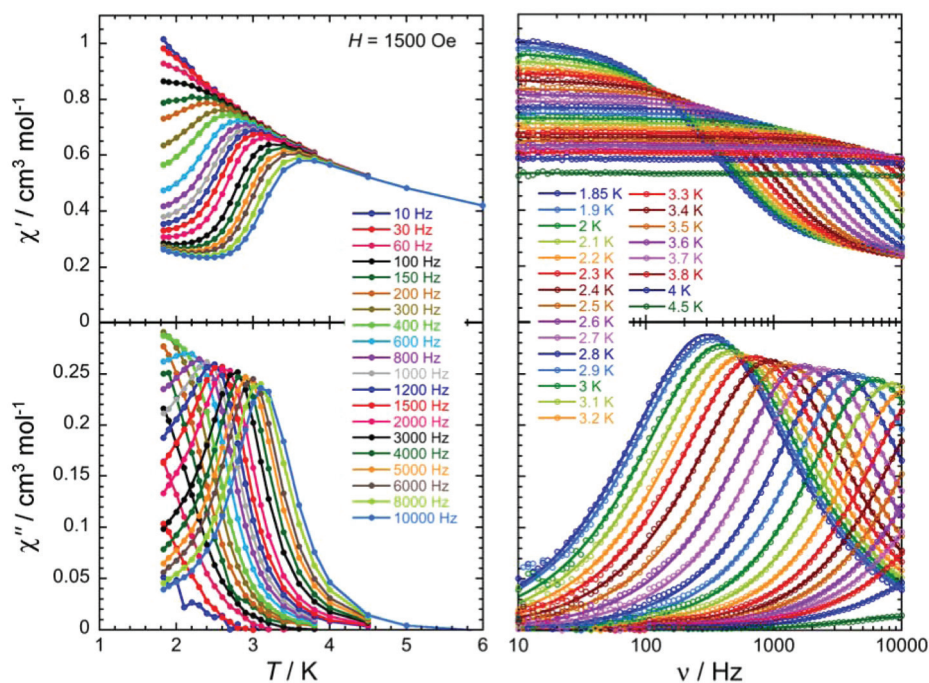
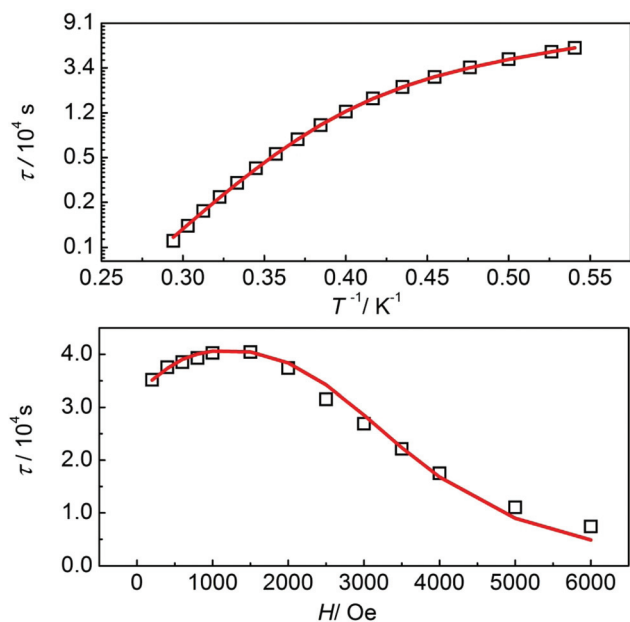


Fig. 9 AC susceptibility data for compound **2** at 1500 DC field in the range 1.85–6 K under driving field frequencies between 10–10 000 Hz. Left: Variable temperatures at different frequencies; full lines are only for eye-guideline. Right: Variable frequency at different temperatures. Full lines: Best fitting according to generalized Debye model (see text).





**Fig. 10** Temperature and field dependence of the magnetization relaxation time as arising from AC magnetic data of compound **2**. Open symbols: Experimental data; red full lines: best fitting according to relaxation mechanisms described in the text.

experimental data becomes possible with three relaxation processes involving Orbach + Raman + Direct mechanisms. This model involved a total number of seven fitting parameters. When any other model is attempt simultaneous fitting of temperature and field relaxation time dependence becomes impossible or are over-parameterized. Best fitting parameters found are:  $U_{\text{eff}}$ : 34 K;  $\tau_0 = 3.8 \times 10^{-10}$  s;  $C = 356 \text{ s}^{-1} \text{ K}^{-n}$ ;  $n = 3.0$ ;  $A_1 = 7.0 \times 10^{-12} \text{ s}^{-1} \text{ Oe}^{-4} \text{ K}^{-1}$ ;  $C_1 = 4.2 \times 10^{-6} \text{ Oe}^{-2}$ ;  $C_2 = 5.3 \times 10^{-6} \text{ Oe}^{-2}$ . The Orbach thermal barrier found is in excellent agreement with the low lying doublets energy levels found from DC magnetic data and also supported by the HF-EPR spectra, if relaxation is considered to be occurring through the first excited doublet arising from the anisotropic exchanged  $S_{\text{eff}} = 1/2$  over the Co(II) sites. The Raman contribution with an  $n$  exponent below 5 can be understood if acoustic phonons are active.<sup>19</sup> The direct and Raman mechanisms determine the field dependence of the relaxation of the magnetization, with at larger fields the direct process becoming dominant. In contrast with complex **1**, the observation of SMM behaviour under applied field in the case of complex **2**, could be attributed to the lesser contribution of transverse components in the Hamiltonian, with a consequent degree of suppression of QTM relaxation pathways. This is supported by the lower  $E/D$  quantum computed values of the Co(II) sites.

## Conclusions

We have successfully prepared and structurally characterized a couple of pivalate based Co(II) complexes. Both of them show strong zero field splitting contribution over the  $S = 3/2$  ground

state that can be modelled under a spin-only formalism, due to a high degree of quenching of the first order orbital momentum contribution. The polynuclear compound **2** exhibits SMM behaviour with an estimated thermal barrier for the Orbach relaxation process of *ca.*  $30 \text{ cm}^{-1}$ . The anisotropic exchange interaction between ground Kramers doublets of each Co(II) site afford a doublet levels ladder that justifies this thermal barrier. DC and AC magnetization data as well as HF-EPR measurements support this description. *Ab initio* correlated CASSCF quantum computations appear in good agreement with experimental results. In spite of the lack of collinearity of the ground doublet  $g$ -tensor of the interacting Co(II) sites, still SMM behaviour is observed in this Co(II)/Co(III) mixed valence polynuclear complex.

## Experimental section

### Material and physical measurements

$[\text{Co}_2(\mu\text{-OH}_2)(\mu\text{-piv})_2(\text{piv})_2(\text{Hpiv})_4]$ , piv = trimethylacetate, was prepared following a previously reported procedure.<sup>12a</sup> All other chemicals were reagent grade and used as receive without further purification. Elemental analysis for C, H and N were performed with a Carlo Erba 1108 analyzer.

**Preparation of complex  $[\text{Co}^{\text{II}}(\text{teaH}_3)_2](\text{piv})_2$  (**1**).** 0.2 g (0.2 mmol) of dinuclear precursor  $[\text{Co}_2(\mu\text{-OH}_2)(\mu\text{-piv})_2(\text{piv})_2(\text{Hpiv})_4]$  were dissolved in 10 ml of acetonitrile at room temperature. To this solution, 0.12 g (0.8 mmol) of teaH<sub>3</sub> (teaH<sub>3</sub> = triethanolamine) were added under vigorous stirring. After complete dissolution the mixture was left undisturbed at room temperature. Very immediately pale orange well shaped single crystals slowly appeared. They were collected by filtration, washed with acetonitrile and air dried. Yield: 0.161 g (72%, Co based).

Anal. Calcd for  $\text{C}_{22}\text{H}_{48}\text{CoN}_2\text{O}_{10}$  (559.56) C: 47.2, H: 8.6, N: 5.0 Found: C: 47.1, H: 8.6, N: 5.0.

**Preparation of complex  $[\text{Co}^{\text{II}}\text{Co}^{\text{III}}(\text{teaH}_3)_2(\text{teaH}_3)(\text{piv})_5(\text{H}_2\text{O})_2]$  (**2**).** 0.2 g (0.2 mmol) of dinuclear precursor  $[\text{Co}_2(\mu\text{-OH}_2)(\mu\text{-piv})_2(\text{piv})_2(\text{Hpiv})_4]$  were dissolved in 10 ml of acetonitrile at room temperature. To this solution, 0.030 g (0.2 mmol) of teaH<sub>3</sub> and 0.020 g (0.2 mmol) of triethylamine were added under vigorous stirring. The resulting mixture was stirred for about half an hour and filtered. It was then left undisturbed at room temperature for slow evaporation. After a couple of days large block dark red crystals of **2** were obtained. They were collected by filtration, washed with acetonitrile and air dried. Yield: 0.0522 g. (43%, Co based).

Anal. Calcd for  $\text{C}_{43}\text{H}_{95}\text{Co}_4\text{N}_3\text{O}_{21}$  (1225.95) C: 42.1, H: 7.8, N: 3.4 Found: C: 42.3, H: 7.4, N: 3.4.

### DC and AC magnetic measurements

The magnetic measurements were carried out in the temperature range between 1.85 and 300 K with applied DC fields ranging from  $-7$  to  $+7$  T, with the use of a MPMS-XL Quantum Design SQUID magnetometer and a PPMS-9 Quantum Design susceptometer. The measurements were performed on a poly-

crystalline sample (11.72 and 15.43 mg for **1** and **2** respectively), covered with immersion oil and enclosed in a sealed polyethylene bag (typical sizes and mass:  $3 \times 0.5 \times 0.02$  cm; 23.42 and 31.34 mg). Prior to the experiments, the field-dependent magnetization was measured at 100 K in order to confirm the absence of any bulk ferromagnetic impurities. The AC susceptibility data have been collected between 10 and 10 000 Hz with AC fields from 1 to 6 Oe and DC fields between 0 and 1 T. The magnetic data were corrected for the diamagnetic contributions from the sample and sample holder.

### High field EPR measurements

High-frequency EPR spectra of pressed powder samples (100–620 GHz) were recorded on a home-built spectrometer.<sup>20</sup> Its radiation source is a 8–20 GHz signal generator (VDI) in combination with an amplifier–multiplier chain (VDI) to obtain the required frequencies. It features a quasi-optical bridge (Thomas Keating) and induction mode detection. The detector is a QMC magnetically tuned InSb hot electron bolometer. The sample is located in an Oxford Instruments 15/17 T cryomagnet equipped with a variable temperature insert (1.5–300 K). The simulations were carried out using the EasySpin package.<sup>21</sup>

### X-ray structure determination

Crystal structures of compounds **1** and **2** were determined with an Oxford Xcalibur, Eos, Gemini CCD area-detector diffractometer using graphite-monochromated Mo-K $\alpha$  radiation ( $\lambda = 0.71069$  Å) at 170 K. Crystals were directly obtained from the synthetic procedure and were picked up prior to filtering and drying. Data was corrected for absorption with CrysAlisPro, Oxford Diffraction Ltd, Version 1.171.33.66, applying an empirical absorption correction using spherical harmonics, implemented in SCALE3 ABSPACK scaling algorithm.<sup>22</sup> The structures were solved by direct methods with SIR97<sup>23</sup> and refined by full-matrix least-squares on  $F^2$  with SHELXL-2014<sup>24</sup> under WinGX platform.<sup>25</sup> Hydrogen atoms were added geometrically and refined as riding atoms with a uniform value of  $U_{\text{iso}}$ . In complex **2** structure, three of the five pivalate methyl groups were found disordered around two positions and were refined with 0.5 : 0.5 fixed occupancy factors.

Final crystallographic data and values of  $R_1$  and  $wR$  are listed in Table 1. CCDC 1812496–1812497† contains the supplementary crystallographic data for this paper.

### Quantum chemical calculations

All calculations reported in this paper were performed with the program package ORCA.<sup>18</sup> For the computation of the exchange interaction, single point calculations for the high-spin state (HS) and the broken symmetry states (BS) at the X-ray geometry were carried out at the B3LYP level of DFT employing the def2-TZVP Ahlrichs basis set for all atoms and the RI (Resolution of Identity) approximation. The SCF calculations were of the spin-polarized type and were tightly converged ( $10^{-7}$  Eh in energy,  $10^{-6}$  in the density change and  $10^{-6}$  in maximum element of the DIIS error vector).

The methodology applied here relies on the broken symmetry formalism, originally developed by Noodleman for SCF methods,<sup>26</sup> which involves a variational treatment within the restrictions of a single spin-unrestricted Slater determinant built upon using different orbitals for different spin. This approach has been later applied within the frame of DFT.<sup>27</sup> The HS (high spin) and BS (broken symmetry) energies were then combined to estimate the exchange coupling parameter  $J$  involved in the widespread used Heisenberg–Dirac–van Vleck Hamiltonian. We have calculated the different spin topologies of broken symmetry nature (see ESI†) by alternatively flipping spin on the different metal sites. The exchange coupling constants  $J_i$  can be obtained after considering the individual pair-like components spin interactions involved in the description of the different broken symmetry states. We used the method proposed by Ruiz and co-workers,<sup>28</sup> where the following equation is applied:

$$E_{\text{BS}} - E_{\text{HS}} = 2J_{12}(2S_1S_2 + S_2), \quad \text{with } S_2 < S_1 \quad (6)$$

In both cases a set of linear equations must be solved to obtain the  $J$  parameters.

The  $g$ -tensors and the zero-field splitting (ZFS) parameters were computed using *ab initio* N-electron valence perturbation theory NEVPT2. State-average complete active space self-consistent (CASSCF) field methods calculations were performed for each Co(II) ions individually (the other Co(II) in the trinuclear complex **2** were modelled as a Zn(II) ion) incorporating the five d-orbitals and seven electrons in the active space (CAS (7,5) setup). Calculations were carried out with the complete set of micro-configurations, 10 quartet and 40 doublet excited states. We have employed TZV basis set for Co(II), Zn(II) and for C, N, O and H atoms we have used SV basis set, in the case of complex **2**. For complex **1** we have used def2-TZVP for all atoms. The calculations utilized the RI approximation and the chain-of spheres (RIJCOSX) approximation to exact exchange as implemented in ORCA. To treat the dynamic correlations, N-electron valence perturbation theory (NEVPT2) calculations on SA-CASSCF converged wave functions were performed. The ZFS parameters were calculated through quasi-degenerate perturbation theory in which an approximation to the Breit–Pauli form of the spin–orbit coupling operator (SOMF) and the effective Hamiltonian theory was utilized. The reported  $g$ -tensors were also computed using the same methodology.

### Conflicts of interest

There are no conflicts of interest to declare.

### Acknowledgements

We gratefully acknowledge UBA, ANPCYT, CONICET, DFG SPP1601, INST 41/863, University of Bordeaux, the Région Nouvelle Aquitaine, the CNRS, the MOLSPIN COST action CA15128 and the GdR MCM-2: Magnétisme et Commutation

Moléculaires for funding resources. PA is a staff member of CONICET. The authors gratefully acknowledge Prof Dr Eva Rentschler for providing access to the computing time granted on the supercomputer Mogon at Johannes Gutenberg University Mainz (hpc.uni-mainz.de).

## References

- (a) G. Christou, D. Gatteschi, D. N. Hendrickson and R. Sessoli, *MRS Bull.*, 2000, **25**, 66–71; (b) D. Gatteschi, R. Sessoli and J. Villain, *Molecular Nanomagnets*, Oxford University Press, 2006.
- (a) R. Sessoli, H.-L. Tsai, A. R. Schake, S. Wang, J. B. Vincent, K. Folting, D. Gatteschi, G. Christou and D. N. Hendrickson, *J. Am. Chem. Soc.*, 1993, **115**, 1804–1816; (b) R. Sessoli, D. Gatteschi, A. Caneschi and M. A. Novak, *Nature*, 1993, **365**, 141–143; (c) D. Gatteschi, A. Caneschi, L. Pardi and R. Sessoli, *Science*, 1994, **265**, 1054–1058.
- (a) M. Affronte, *J. Mater. Chem.*, 2009, **19**, 1731–1737; (b) M. Mannini, F. Pineider, P. Sainctavit, C. Danieli, E. Otero, C. Sciancalepore, A. M. Talarico, M. A. Arrio, A. Cornia, D. Gatteschi and R. Sessoli, *Nat. Mater.*, 2009, **8**, 194–197.
- (a) M. N. Leuenberger and D. Loss, *Nature*, 2001, **410**, 789–793; (b) J. Lehmann, A. Gaita-Ariño, E. Coronado and D. Loss, *J. Mater. Chem.*, 2009, **19**, 1672–1677; (c) F. Troiani and M. Affronte, *Chem. Soc. Rev.*, 2011, **40**, 3119–3129; (d) G. Aromí, D. Aguilà, P. Gamez, F. Luis and O. Roubeau, *Chem. Soc. Rev.*, 2012, **41**, 537–546.
- (a) L. Bogani and W. Wernsdorfer, *Nat. Mater.*, 2008, **7**, 179–186; (b) S. Sanvito, *Chem. Soc. Rev.*, 2011, **40**, 3336–3355.
- (a) M. Evangelisti and E. K. Brechin, *Dalton Trans.*, 2010, **39**, 4672; (b) J.-L. Liu, Y.-C. Chen, F.-S. Guo and M.-L. Tong, *Coord. Chem. Rev.*, 2014, **281**, 26–49; (c) Y.-Z. Zheng, G.-J. Zhou, Z. Zheng and R. E. P. Winpenny, *Chem. Soc. Rev.*, 2014, **43**, 1462–1475.
- (a) G. Aromí and E. K. Brechin, in *Single-Molecule Magnets and Related Phenomena*, ed. R. Winpenny, 2006, vol. 122, pp. 1–67; (b) *Molecular Nanomagnets and Related Phenomena*, ed. S. Gao, Structure and Bonding, Springer Berlin Heidelberg, Berlin, Heidelberg, 2015, vol. 164.
- M. Murrie, *Chem. Soc. Rev.*, 2010, **39**, 1986–1995.
- (a) E. Colacio, J. Ruiz, E. Ruiz, E. Cremades, J. Krzystek, S. Carretta, J. Cano, T. Guidi, W. Wernsdorfer and E. K. Brechin, *Angew. Chem., Int. Ed.*, 2013, **52**, 9130–9134; (b) D.-K. Cao, J.-Q. Feng, M. Ren, Y.-W. Gu, Y. Song and M. D. Ward, *Chem. Commun.*, 2013, **49**, 8863–8865; (c) L. Chen, J. Wang, J. Wei, W. Wernsdorfer, X. Chen, Y. Zhang, Y. Song and Z. Xue, *J. Am. Chem. Soc.*, 2014, **136**, 12213–12216; (d) R. Ruamps, L. J. Batchelor, R. Guillot, G. Zakhia, A.-L. Barra, W. Wernsdorfer, N. Guihéry and T. Mallah, *Chem. Sci.*, 2014, **5**, 3418; (e) E. Carl, S. Demeshko, F. Meyer and D. Stalke, *Chem. – Eur. J.*, 2015, **2**, 10109–10115; (f) V. V. Novikov, A. A. Pavlov, Y. V. Nelyubina, M. Boulon, O. A. Varzatskii, Y. Z. Voloshin and R. E. P. Winpenny, *J. Am. Chem. Soc.*, 2015, **137**, 9792–9795; (g) F. Shao, B. Cahier, N. Guihéry, E. Rivière, R. Guillot, A.-L. Barra, Y. Lan, W. Wernsdorfer, V. E. Campbell and T. Mallah, *Chem. Commun.*, 2015, **51**, 16475–16478; (h) S. Vaidya, A. Upadhyay, S. K. Singh, T. Gupta, S. Tewary, S. K. Langley, J. P. S. Walsh, K. S. Murray, G. Rajaraman and M. Shanmugam, *Chem. Commun.*, 2015, **2**, 3–6; (i) Y.-Z. Zhang, S. Gómez-Coca, A. J. Brown, M. R. Saber, X. Zhang and K. R. Dunbar, *Chem. Sci.*, 2016, **7**, 6519–6527; (j) T. J. Woods, M. F. Ballesteros-Rivas, S. Gómez-Coca, E. Ruiz and K. R. Dunbar, *J. Am. Chem. Soc.*, 2016, **138**, 16407–16416; (k) Y.-F. Deng, Z. Wang, Z. Ouyang, B. Yin, Z. Zheng and Y. Zheng, *Chem. – Eur. J.*, 2016, **22**, 14821–14825; (l) Y. Rechkemmer, F. D. Breitgoff, M. van der Meer, M. Atanasov, M. Hakl, M. Orlita, P. Neugebauer, F. Neese, B. Sarkar and J. van Slageren, *Nat. Commun.*, 2016, **7**, 10467; (m) A. K. Mondal, J. Jover, E. Ruiz and S. Konar, *Chem. Commun.*, 2017, 5338–5341; (n) X.-N. Yao, J.-Z. Du, Y.-Q. Zhang, X.-B. Leng, M.-W. Yang, S.-D. Jiang, Z.-X. Wang, Z.-W. Ouyang, L. Deng, B.-W. Wang and S. Gao, *J. Am. Chem. Soc.*, 2017, **139**, 373–380; (o) X.-N. Yao, M.-W. Yang, J. Xiong, J.-J. Liu, C. Gao, Y.-S. Meng, S.-D. Jiang, B.-W. Wang and S. Gao, *Inorg. Chem. Front.*, 2017, **4**, 701–705.
- (a) H. Oshio and M. Nakano, *Chem. – Eur. J.*, 2005, **11**, 5178–5185; (b) J. Cirera, E. Ruiz, S. Alvarez, F. Neese and J. Kortus, *Chem. – Eur. J.*, 2009, **15**, 4078–4087; (c) R. Ruamps, R. Maurice, C. de Graaf and N. Guihéry, *Inorg. Chem.*, 2014, **53**, 4508–4516.
- A. V. Funes, L. Carrella, L. Sorace, E. Rentschler and P. Alborés, *Dalton Trans.*, 2015, **44**, 2390–2400.
- (a) G. Aromí, A. S. Batsanov, P. Christian, M. Helliwell, A. Parkin, S. Parsons, A. A. Smith, G. A. Timco and R. E. P. Winpenny, *Chem. – Eur. J.*, 2003, 5142–5161; (b) P. Alborés and E. Rentschler, *Angew. Chem., Int. Ed.*, 2009, **48**, 9366–9370; (c) I. C. Lazzarini, L. Carrella, E. Rentschler and P. Alborés, *Polyhedron*, 2012, **31**, 779–788; (d) I. C. Lazzarini, A. V. Funes, L. Carrella, L. Sorace, E. Rentschler and P. Alborés, *Eur. J. Inorg. Chem.*, 2014, **2014**, 2561–2568.
- S. Alvarez, P. Alemany, D. Casanova, J. Cirera, M. Lluell and D. Avnir, *Coord. Chem. Rev.*, 2005, **249**, 1693–1708.
- A. J. Ward, M. Burger, C. Aquino, J. K. Clegg, P. Turner, A. F. Masters and T. Maschmeyer, *Acta Crystallogr., Sect. E: Struct. Rep. Online*, 2006, **62**, m2429–m2431.
- F. Lloret, M. Julve, J. Cano, R. Ruiz-García and E. Pardo, *Inorg. Chim. Acta*, 2008, **361**, 3432–3445.
- N. F. Chilton, R. P. Anderson, L. D. Turner, A. Soncini and K. S. Murray, *J. Comput. Chem.*, 2013, **34**, 1164–1175.
- (a) V. Tudor, A. Madalan, V. Lupu, F. Lloret, M. Julve and M. Andruh, *Inorg. Chim. Acta*, 2010, **363**, 823–826; (b) T. Shiga and H. Oshio, *Polyhedron*, 2007, **26**, 1881–1884; (c) M. Moragues-Canovas, C. E. Talbot-Eeckelaers,

- L. Catala, F. Lloret, W. Wernsdorfer, E. K. Brechin and T. Mallah, *Inorg. Chem.*, 2006, **45**, 7038–7040; (d) R. Tirfoin, L.-M. Chamoreau, Y. Li, B. Fleury, L. Lisnard and Y. Journaux, *Dalton Trans.*, 2014, **43**, 16805–16817; (e) S. Schmitz, K. Y. Monakhov, J. van Leusen, N. V. Izarova, V. Heß and P. Kögerler, *RSC Adv.*, 2016, **6**, 100664–100669; (f) F.-L. Yang, F. Shao, G.-Z. Zhu, Y.-H. Shi, F. Gao and X.-L. Li, *ChemistrySelect*, 2017, **2**, 110–117.
- 18 F. Neese, *Wiley Interdiscip. Rev.: Comput. Mol. Sci.*, 2012, **2**, 73–78.
- 19 K. N. Shrivastava, *Phys. Status Solidi*, 1972, **51**, 377–387.
- 20 P. Neugebauer, D. Bloos, R. Marx, P. Lutz, M. Kern, D. Aguilà, J. Vaverka, O. Laguta, C. Dietrich, R. Clérac and J. van Slageren, *Phys. Chem. Chem. Phys.*, 2018, **20**, 15528–15534.
- 21 S. Stoll and A. Schweiger, *J. Magn. Reson.*, 2006, **178**, 42.
- 22 *SCALE3 ABSPACK: Empirical absorption correction, CrysAlis – Software package*, 2006.
- 23 A. Altomare, M. C. Burla, M. Camalli, G. L. Cascarano, C. Giacovazzo, A. Guagliardi, A. G. G. Moliterni, G. Polidori and R. Spagna, *J. Appl. Crystallogr.*, 1999, **32**, 115–119.
- 24 G. M. Sheldrick, *Acta Crystallogr., Sect. A: Found. Crystallogr.*, 2008, **64**, 112–122.
- 25 L. J. Farrugia, *J. Appl. Crystallogr.*, 2012, **45**, 849–854.
- 26 L. Noodleman, *J. Chem. Phys.*, 1981, **74**, 5737–5743.
- 27 L. Noodleman and E. J. Baerends, *J. Am. Chem. Soc.*, 1984, **106**, 2316–2327.
- 28 E. Ruiz, J. Cano, S. Alvarez and P. Alemany, *J. Comput. Chem.*, 1999, **20**, 1391–1400.